The Astrophysical Journal, 678:1032–1041, 2008 May 10

THE c2d *SPITZER* SPECTROSCOPIC SURVEY OF ICES AROUND LOW-MASS YOUNG STELLAR OBJECTS. III. CH_4

Karin I. Öberg,[1] A. C. Adwin Boogert,[2] Klaus M. Pontoppidan,[3] Geoffrey A. Blake,[3]
Neal J. Evans,[4] Fred Lahuis,[5] and Ewine F. van Dishoeck[1]
Received 2007 October 15; accepted 2008 January 7

ABSTRACT

CH_4 is proposed to be the starting point of a rich organic chemistry. Solid CH_4 abundances have previously been determined mostly toward high-mass star-forming regions. *Spitzer* IRS now provides a unique opportunity to probe solid CH_4 toward low-mass star-forming regions as well. Infrared spectra from the *Spitzer Space Telescope* are presented to determine the solid CH_4 abundance toward a large sample of low-mass young stellar objects. A total of 25 out of 52 ice sources in the "Cores to Disks" (c2d) Legacy program have an absorption feature at 7.7 μm, attributed to the bending mode of solid CH_4. The solid CH_4/H_2O abundances are 2%–8%, except for three sources with abundances as high as 11%–13%. The latter sources have relatively large uncertainties due to small total ice column densities. Toward sources with H_2O column densities above 2×10^{18} cm^{-2}, the CH_4 abundances (20 out of 25) are nearly constant at 4.7% $\pm$ 1.6%. Correlation plots with solid H_2O, CH_3OH, CO_2, and CO column densities and abundances relative to H_2O reveal a closer relationship of solid CH_4 with CO_2 and H_2O than with solid CO and CH_3OH. The inferred solid CH_4 abundances are consistent with models where CH_4 is formed through sequential hydrogenation of C on grain surfaces. Finally, the equal or higher abundances toward low-mass young stellar objects compared with high-mass objects and the correlation studies support this formation pathway as well, but not the two competing theories: formation from CH_3OH and formation in gas phase with subsequent freezeout.

Subject headings: astrochemistry — infrared: ISM — ISM: abundances — ISM: molecules — stars: formation

1. INTRODUCTION

The presence and origin of complex organic molecules in protostellar regions and their possible incorporation into protoplanetary disks are active topics of research. CH_4 is proposed to be a starting point of a rich chemistry, especially when UV photons are present (Dartois et al. 2005). In particular, CH_4 is believed to play a key role in the formation process of prebiotic molecules (Markwick et al. 2000).

CH_4 is less well studied in interstellar and circumstellar media compared to other small organic molecules because CH_4 has no permanent dipole moment and therefore cannot be observed by pure rotational transitions at radio wavelengths. Solid CH_4 was first detected through its bending mode at 7.67 μm from the ground by Lacy et al. (1991) and with the *Infrared Space Observatory* Short Wavelength Spectrometer (*ISO* SWS) by Boogert et al. (1996) toward a few high-mass sources. Tentative claims have been made toward some other objects, including low-mass protostars, but are inconclusive because of the low signal-to-noise ratio (S/N) of these data (Cernicharo et al. 2000; Gürtler et al. 2002; Alexander et al. 2003). Solid CH_4 has also been detected from the ground through its stretching mode at 3.3 μm, but only toward the brightest high-mass sources due to problems in removing the many atmospheric lines in this spectral region (Boogert et al. 2004a).

Models predict CH_4 to form rapidly on cool grains through successive hydrogenation of atomic C; similarly, H_2O is formed through hydrogenation of atomic O (van de Hulst 1946; Allen & Robinson 1977; Tielens & Hagen 1982; Brown et al. 1988; Hasegawa et al. 1992; Aikawa et al. 2005). Observations of CH_4 hence provide insight into the basic principles of grain surface chemistry. Compared to H_2O, the observed gas- and solid-state CH_4 abundances are low; reported CH_4 abundances are typically a few percent with respect to H_2O (Lacy et al. 1991; Boogert et al. 1998). This points to relatively low atomic C abundances at the time of CH_4 formation, with most C already locked up in CO as H readily reacts with C on surfaces (Hiraoka et al. 1998). This is in agreement with the high CH_3OH abundances in several lines of sight, formed by hydrogenation of CO (Dartois et al. 1999; Pontoppidan et al. 2003), and large CO_2 abundances, formed through oxidation of CO or hydrogenated CO. That these molecules are all formed through a similar process is corroborated by the profiles of solid CO_2 absorption bands, which usually show an intimate mixture of CO_2, CH_3OH, and H_2O in interstellar ices (Gerakines et al. 1999; Boogert et al. 2000; Knez et al. 2005).

If CH_4 is formed efficiently through grain surface reactions as well, CH_4 should be similarly mixed with H_2O. Observations of solid CH_4 toward a few high-mass young stellar objects (YSOs) show that the CH_4 absorption band profiles are broad and agree better with CH_4 in a hydrogen-bonding ice, H_2O or CH_3OH, than with a pure CH_4 ice or CH_4 mixed with CO (Boogert et al. 1997). This profile analysis does not, however, exclude CH_4 formation from photoprocessing of CH_3OH (Allamandola et al. 1988; Gerakines et al. 1996). In addition, because of the small sample in previous studies, it is unclear if these broad profiles are a universal feature. Hence, it cannot be excluded that CH_4 in some environments may form in the gas phase and subsequently freeze out.

Because formation pathway efficiency depends on environment, another method for testing formation routes is through exploring the distribution of CH_4 toward a large sample of objects of different ages, luminosities, and ice column densities. In

[1] Leiden Observatory, Leiden University, NL 2300 RA Leiden, Netherlands; oberg@strw.leidenuniv.nl.
[2] IPAC, NASA Herschel Science Center, California Institute of Technology, Pasadena, CA 91125.
[3] Division of Geological and Planetary Sciences, California Institute of Technology, Pasadena, CA 91125.
[4] Department of Astronomy, University of Texas at Austin, Austin, TX 78712-0259.
[5] SRON, NL 9700 AV Groningen, Netherlands.

TABLE 1
SOURCE SAMPLE OF 25 LOW-MASS STARS OBSERVED WITH *Spitzer* IRS

Source	Alias	R.A. (J2000.0)	Decl. (J2000.0)	Cloud	Type	ObsID
IRAS 03235+3004		03 26 37.5	+30 15 27.9	Perseus	Low	9835520
IRAS 03245+3002		03 27 39.0	+30 12 59.3	Perseus	Low	6368000
L1455 SMM 1		03 27 43.3	+30 12 28.8	Perseus	Low	15917056
IRAS 03254+3050		03 28 34.2	+31 00 51.2	Perseus	Low	11827200
B1-c		03 33 17.9	+31 09 31.0	Perseus	Low	13460480
B1-b		03 33 20.3	+31 07 21.4	Perseus	Low	1596544
L1489 IRS	IRAS 04016+2610	04 04 43.1	+26 18 56.4	Taurus	Low	3528960
IRAS 08242−5050	HH 46 IRS	08 25 43.8	−51 00 35.6	HH 46	Low	5638912
IRAS 12553−7651		12 59 06.6	−77 07 40.0	Cha	Low	9830912
IRAS 15398−3359		15 43 02.3	−34 09 06.7	B228	Low	5828864
GSS 30 IRS 1		16 26 21.4	−24 23 04.1	Ophiuchus	Low	12699392
IRS 42		16 27 21.5	−24 41 43.1	Ophiuchus	Low	12699648
IRS 43		16 27 27.0	−24 40 52.0	Ophiuchus	Low	12699648
IRS 44		16 27 28.1	−24 39 35.0	Ophiuchus	Low	12699648
IRS 63		16 31 35.7	−24 01 29.5	Ophiuchus	Low	12676608
VSSG 17	IRS 47	16 27 30.2	−24 27 43.4	Ophiuchus	Low	12698624
RNO 91	IRAS 16316−1540	16 34 29.3	−15 47 01.4	L43	Low	5650432
B59 YSO 5		17 11 22.2	−27 26 02.3	B59	Low	14894336
2MASS J17112317−2724315		17 11 23.1	−27 24 32.6	B59	Low	14894592
SVS 4-5	EC 88	18 29 57.6	+01 13 00.6	Serpens	Low	9407232
EC 92	SVS 4-10	18 29 57.9	+0.1 12 51.6	Serpens	Low	9407232
CrA IRS 5		19 01 48.0	−36 57 21.6	Corona Australis	Low	9835264
CrA IRS 7B		19 01 56.4	−36 57 28.0	Corona Australis	Low	9835008
CrA IRAS 32		19 02 58.7	−37 07 34.5	Corona Australis	Low	9832192
L1014 IRS		21 24 07.5	+49 59 09.0	L1014	Low	12116736
W33A		18 14 39.4	−17 52 01.3		High	32900920
NGC 7538 IRS 9		23 14 01.6	+61 27 20.2		High	09801532
GL 989		06 41 10.1	+0.9 29 35.8		High	71602619
GL 7009S		18 34 20.9	−05 59 42.2		High	15201140

NOTES.—Units of right ascension are hours, minutes, and seconds, and units of declination are degrees, arcminutes, and arcseconds. In addition, four high-mass stars with previously published *ISO* spectra and CH_4 detections are included for comparison.

addition, correlations, or lack thereof, with other ice constituents may provide important clues to how the molecule is formed. If CH_4 is formed through hydrogenation on grain surfaces in quiescent clouds, the CH_4 abundance with respect to H_2O should be fairly source independent since this mechanism mainly depends on the initial conditions of the cloud before the star forms, which seem to vary little between different star-forming regions. Because of the generality of this mechanism, the CH_4 and H_2O, and possibly CO_2, column densities should correlate over a large range of different environments. This is also the prediction of several models where the solid CH_4/H_2O and CH_4/CO_2 ratios in dark clouds vary little as a function of both time (Hasegawa et al. 1992) and distance into a cloud that has collapsed (Aikawa et al. 2005). In contrast, CO, which is formed in the gas phase and subsequently frozen out, is predicted to only correlate with CH_4 during certain time intervals. If CH_4 instead forms in the gas phase, solid CH_4 should be better correlated with solid CO than with solid H_2O and CO_2, since pure CH_4 freezes out and desorbs at similar temperatures to CO (Collings et al. 2004). Finally, if CH_4 forms by UV photoprocessing of CH_3OH, more CH_4 would also be expected to form toward sources with stronger UV fields, i.e., higher mass objects.

The objective of this study is to determine the CH_4 abundances and distribution pattern toward a sample of low-mass YSOs, varying in evolutionary stage and total ice column density. The distribution pattern and correlations with other ice constituents within the sample, as well as comparison with high-mass YSOs, will be used to constrain the CH_4 formation mechanism. This study is based on spectra acquired with the *Spitzer* Infrared Spectrometer (IRS) as part of our legacy program "From Molecular Cores to Protoplanetary Disks" (c2d), which provides a large sample (41 sources) of infrared spectra of low-mass star formation regions (Evans et al. 2003). In addition, 11 sources are added from the GTO program 2 for which ground-based 3–5 μm observations already exist (Pontoppidan et al. 2003). Overviews of the H_2O, CO_2, CH_3OH, and other ice species in these data are found in Boogert et al. (2008, hereafter Paper I) and Pontoppidan et al. (2008, hereafter Paper II). The detection of solid CH_4 toward one of the sources, HH 46 IRS, was published by Boogert et al. (2004b). We have detected an absorption feature, which is attributed to solid CH_4, toward 25 out of 52 low-mass ice sources found in this c2d sample.

2. SOURCE SAMPLE SELECTION, OBSERVATIONS, AND DATA REDUCTION

The source sample consists of a combination of known low-mass protostars and new protostars discovered by their *Spitzer* IRAC and MIPS broadband spectral energy distributions. *Spitzer* IRS spectra were obtained as part of the c2d Legacy program (PIDs 172 and 179), as well as a dedicated open time program (PID 20604) and a few archival spectra observed as a part of the GTO programs (PID 2). Among the targets observed with the IRS Short-Long (SL) module, 41 ice sources were identified from their spectra in the c2d sample (Paper I). The GTO sources are all associated with the Ophiuchus cloud and were selected based on previous ice observations at 3–5 μm (Pontoppidan et al. 2003). The source sample of 25 low-mass protostars presented

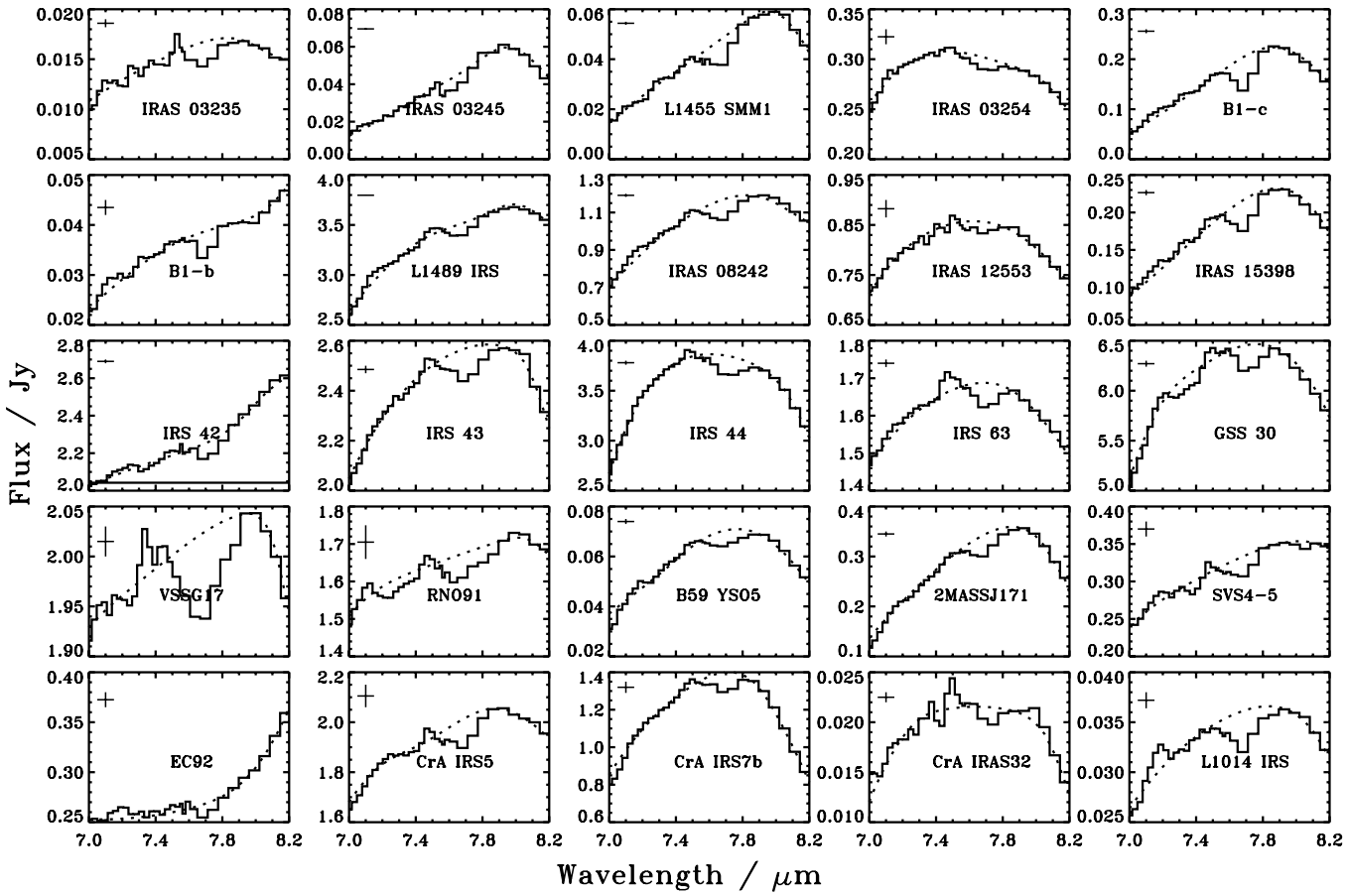

FIG. 1.—*Spitzer* IRS spectra (*solid line*) of the CH_4 sources between 7.0 and 8.2 μm, plotted together with the chosen spline continua (*dotted line*). The tick bar in the upper left corner indicates the noise level derived within the c2d pipeline.

here was selected from the 41 c2d and 11 GTO ice sources based solely on the existence of an absorption feature at 7.7 μm, identified with solid CH_4 (Table 1). Due to the high sensitivity of the *Spitzer* IRS, a large range of star formation stages are represented in the sample from very young YSOs at the interface of the Class 0/I stages (e.g., B1-c) to objects like RNO 91, identified as an inclined disk with a remnant envelope. It also includes very low luminosity objects (VELLOs) such as L1014 IRS (Young et al. 2004). More information about the evolutionary stages of the objects is reported in Paper I.

The *Spitzer* IRS spectra were reduced using the two-dimensional basic calibrated data (BCD) spectral images, produced by the *Spitzer* Science Center (SSC) pipeline version S13.2.0, as a starting point. The low-resolution modules, which are the relevant ones for the solid CH_4 feature, were reduced in a similar way to ground-based spectra. First, the spectral and spatial dimensions were orthogonalized, and then the two-dimensional images of the two nodding positions were subtracted in order to remove the extended emission. A fixed width extraction was performed and then the one-dimensional spectra were averaged. Subsequently, the spectra were divided by spectra of the standard star HR 2194, reduced in the same way, to correct for wavelength-dependent slit losses. Finally, the spectra were multiplied along the flux scale in order to match *Spitzer* IRAC photometry. One source, EC 92, was carefully extracted manually due to multiple other sources present in the slit. More details about the reduction and the complete mid-infrared spectra of the c2d sources are presented in Paper I. The CH_4 7.7 μm absorption feature falls within the range of the IRS modules SL1 and SL2. At these wavelengths the resolving power $R = \lambda/\Delta\lambda$ of IRS is 65 or 0.12 μm for SL1 and 125 or 0.06 μm for SL2 (IRS Data Handbook). The plotted spectra are made up using data from the main orders of SL1 and SL2, while the SL1 bonus order was only used to confirm detections. SL2 stops around 7.6 μm so the peak of the CH_4 absorption feature is always in SL1. The part of the spectra from the SL2 module is hence mainly used to determine the continuum and in some cases the shape of a low-wavelength wing. When comparing observations to laboratory spectra, the laboratory spectra are always convolved to the resolution of SL1 (0.12 μm, sampled with 2 pixels per resolution element).

ISO SWS spectra of four high-mass YSOs are used for comparison between low- and high-mass protostars in this paper. The latest standard processed data (SPD) pipeline version 10.1 products were taken from the *ISO* archive, and the detector scans were cleaned from cosmic-ray hits and averaged. The final spectra do not show significant differences with respect to the data published in Keane et al. (2001).

3. RESULTS

3.1. CH_4 *Column Densities*

Figure 1 shows the flux-calibrated spectra of the 25 low-mass YSOs containing the CH_4 7.7 μm absorption feature. The spectra were converted to optical depth scale using a smooth spline continuum fitted to the 7–7.4 and 8.0–8.3 μm regions as shown in Figure 1. A local continuum is necessary since the CH_4 feature lies on the edge of other broader features such as the 9.7 μm feature. Fitting the continuum is complicated by the presence of

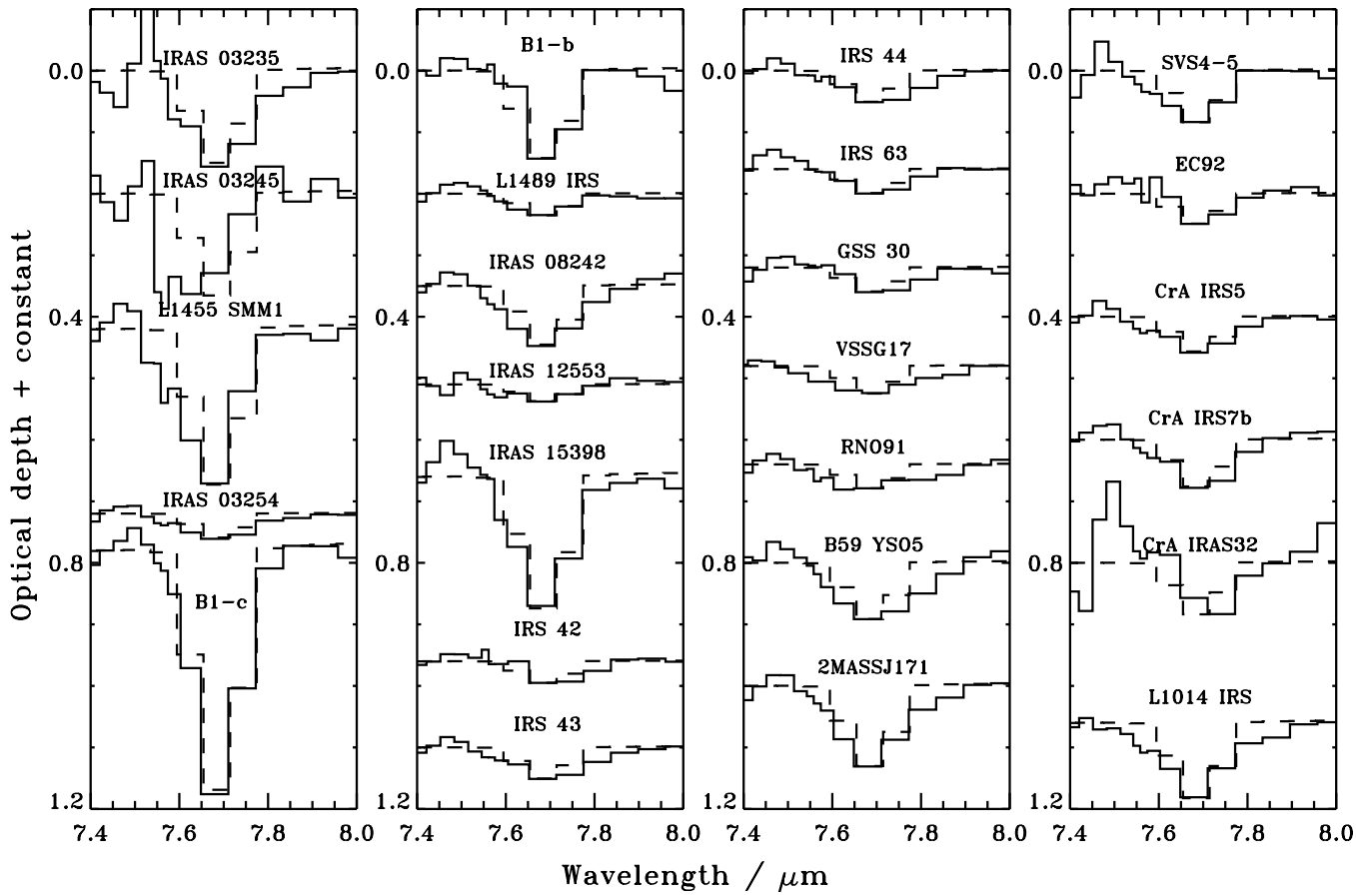

FIG. 2.—Optical depth spectra of the CH_4 sources plotted together with laboratory spectra (*dashed line*) of a $CH_4 : H_2O = 1 : 3$ mixture (Leiden databases at http://www.strw.leidenuniv.nl/~lab/databases) convolved to at the same resolution and sampled in the same way as the observational data.

a weak H I recombination emission line at 7.5 μm (Pfα) toward several of the sources, e.g., the CrA sources, IRAS 03235+3004, L1489 IRS, RNO 91, and SVS 4-5. Of these ground-based spectra, around 4 μm exist for CrA IRS 5, CrA IRS 7B, IRAS 03235+3004, L1489 IRS, and SVS 4-5. In all of these spectra the 4.05 μm H I Brα is clearly visible, corroborating the identification of the emission feature with hydrogen.

To estimate the uncertainties introduced by the choice of continuum, the spectra were also converted to optical depth scale by adopting a local, straight line continuum between 7.4 and 7.9 μm. The differences in optical depth using the two different continua are less than 20% for most sources, but between 30% and 60% for a few cases: CrA IRS 7B, IRAS 03235+3004, IRAS 12553−7651, and RNO 91. The resulting optical depth spectra using the smooth spline continuum subtraction are shown in Figure 2.

The peak position, FWHM, and peak optical depth of the 7.7 μm absorption feature along each line of sight were calculated from the best Gaussian fit between 7.5 and 7.9 μm (Table 2). The reported error estimates include uncertainties in the fit and choice of continuum. The typical peak position is 7.69 μm, and the peak widths range from 0.07 to 0.27 μm. The features hence range from unresolved to barely resolved as the resolution at the center peak position is 0.12 μm. The large widths of the feature in the observed spectra, except for B1-b, suggest that CH_4 is generally in an H_2O- or CH_3OH-dominated mixture, where laboratory data show that the CH_4 feature has a width of up to 0.15 μm (Boogert et al. 1997).

Figure 3 compares the source with the deepest absorption feature, B1-c, with different CH_4 containing laboratory ice spectra, convolved to the resolution of IRS-SL1. In the three laboratory ice spectra used here—an H_2O-dominated ice, an ice mixture that contains equal parts of H_2O, CH_3OH, and CO_2, and pure CH_4, all at 10 K—the CH_4 absorption profile has both different widths and peak positions. Toward most sources, as for B1-c, H_2O-dominated ice spectra provide the best fit. Hence, comparisons with an $H_2O : CH_4 = 3 : 1$ ice spectrum were used to determine the amount of CH_4 present in the observed spectra and also how much of the 7.7 μm feature can be accounted for by solid CH_4 (Fig. 2). Table 2 shows that CH_4 can account for 45%–100% of the absorption.

The CH_4 column densities were calculated from the integrated optical depths of the laboratory spectra, scaled to the peak optical depths of the observations, and the band strength for the bending mode of solid CH_4 in an H_2O rich ice, 4.7×10^{-18} cm molecule^{-1} (Boogert et al. 1997). The uncertainty in CH_4 column densities stems from both the baseline subtraction and the uncertainty in ice mixture composition even after an H_2O-rich ice has been assumed. To obtain abundances with respect to solid H_2O, the CH_4 column densities were divided by the solid H_2O column densities from Paper I. Figure 4 shows the CH_4 abundances with respect to H_2O as a function of H_2O column density. The CH_4 abundances in the entire sample vary between 2% and 13%, and it is seen in the plot that the sample can be split into two parts: sources with H_2O column densities around 2×10^{18} cm^{-2} and sources with H_2O column densities of $(3–40) \times 10^{18}$ cm^{-2}. In the former group the CH_4 abundances with respect to H_2O vary between 6% and 13%, and in the latter group all CH_4 abundances fall between 2% and 8%. Due to the low total column densities

TABLE 2

GAUSSIAN PARAMETERS OF THE OBSERVED ABSORPTION FEATURES AND THE CH_4 COLUMN DENSITIES AND ABUNDANCES RELATIVE TO SOLID H_2O AND UPPER LIMITS OF SO_2

Source	λ (μm)	FWHM (μm)	τ_{peak}	$\int \tau_{7.7}$ (cm^{-1})	$\int \tau_{CH_4}$ (cm^{-1})	$N(CH_4)$ (10^{17} cm^{-2})	$N(CH_4)/N(H_2O) \times 100$	$N(SO_2)_{max}/N(H_2O) \times 100$
IRAS 03235+3004	7.69 ± 0.03	0.16 ± 0.05	0.16 ± 0.07	4.6 ± 1.0	2.9 ± 0.8	6.2 ± 1.8	4.3 ± 1.4	0.35 ± 0.19
IRAS 03245+3002	7.59 ± 0.03	0.20 ± 0.08	0.17 ± 0.04	4.3 ± 0.1	3.2 ± 0.4	6.8 ± 0.8	1.7 ± 0.3	0.08 ± 0.01
L1455 SMM 1	7.66 ± 0.01	0.15 ± 0.02	0.24 ± 0.03	6.2 ± 0.3	4.9 ± 0.1	10. ± 0.1	5.8 ± 0.9	0.21 ± 0.03
IRAS 03254+3050	7.68 ± 0.01	0.20 ± 0.03	0.040 ± 0.008	1.4 ± 0.2	0.7 ± 0.1	1.6 ± 0.3	4.0 ± 0.9	0.45 ± 0.14
B1-c	7.68 ± 0.01	0.13 ± 0.01	0.40 ± 0.05	8.7 ± 1.3	7.6 ± 1.2	16 ± 3	5.4 ± 1.4	0.11 ± 0.03
B1-b	7.70 ± 0.01	0.10 ± 0.01	0.16 ± 0.01	2.7 ± 0.1	2.8 ± 0.1	5.9 ± 0.2	3.3 ± 0.6	0.00 ± 0.01
L1489 IRS	7.68 ± 0.01	0.13 ± 0.01	0.037 ± 0.006	0.93 ± 0.04	0.64 ± 0.04	1.4 ± 0.1	3.1 ± 0.2	0.14 ± 0.01
IRAS 08242−5050	7.68 ± 0.06	0.17 ± 0.16	0.098 ± 0.063	2.9 ± 1.8	1.9 ± 0.8	3.9 ± 1.8	5.0 ± 2.4	0.40 ± 0.68
IRAS 12553−7651	7.66 ± 0.02	0.18 ± 0.04	0.026 ± 0.005	0.6 ± 0.1	0.5 ± 0.1	1.1 ± 0.1	3.8 ± 0.9	0.13 ± 0.03
IRAS 15398−3359	7.68 ± 0.01	0.13 ± 0.01	0.22 ± 0.03	5.1 ± 0.6	4.2 ± 0.8	8.8 ± 1.7	6.0 ± 2.0	0.20 ± 0.06
IRS 42	7.72 ± 0.01	0.12 ± 0.03	0.041 ± 0.012	0.82 ± 0.11	0.62 ± 0.22	1.4 ± 0.4	7.7 ± 2.4	0.21 ± 0.06
IRS 43	7.70 ± 0.01	0.21 ± 0.04	0.050 ± 0.014	1.7 ± 0.6	0.94 ± 0.33	2.1 ± 0.6	6.6 ± 2.3	0.70 ± 0.36
IRS 44	7.71 ± 0.01	0.19 ± 0.01	0.053 ± 0.015	1.7 ± 0.4	0.9 ± 0.2	2.1 ± 0.4	6.1 ± 1.4	0.63 ± 0.23
IRS 63	7.70 ± 0.14	0.14 ± 0.13	0.042 ± 0.026	1.0 ± 0.4	0.72 ± 0.31	1.6 ± 0.7	7.9 ± 3.8	0.42 ± 0.59
GSS 30	7.72 ± 0.16	0.14 ± 0.13	0.045 ± 0.027	1.1 ± 0.8	0.7 ± 0.4	1.6 ± 0.9	11 ± 6.2	0.60 ± 0.9
VSSG 17	7.68 ± 0.01	0.26 ± 0.04	0.042 ± 0.006	1.8 ± 0.2	0.8 ± 0.1	1.8 ± 0.2	11 ± 2.2	1.5 ± 0.35
RNO 91	7.69 ± 0.03	0.27 ± 0.13	0.038 ± 0.009	1.6 ± 0.7	0.68 ± 0.17	1.6 ± 0.5	4.8 ± 1.6	0.76 ± 0.44
B59 YSO 5	7.70 ± 0.01	0.19 ± 0.06	0.096 ± 0.050	3.2 ± 3.4	1.8 ± 0.9	3.8 ± 2.0	2.7 ± 1.6	0.31 ± 0.37
2MASS J17112317	7.69 ± 0.01	0.17 ± 0.06	0.13 ± 0.052	3.9 ± 2.0	2.5 ± 1.0	5.4 ± 2.2	2.8 ± 1.2	0.20 ± 0.23
SVS 4-5	7.67 ± 0.01	0.16 ± 0.02	0.083 ± 0.010	2.2 ± 0.2	1.6 ± 0.3	3.5 ± 0.6	6.1 ± 1.7	0.29 ± 0.08
EC 92	7.71 ± 0.01	0.07 ± 0.10	0.066 ± 0.032	0.67 ± 0.21	0.88 ± 0.47	2.0 ± 1.2	13 ± 7.7	0.33 ± 0.23
CrA IRS 5	7.68 ± 0.01	0.19 ± 0.02	0.055 ± 0.011	1.7 ± 0.3	1.1 ± 0.1	2.3 ± 0.3	6.2 ± 1.0	0.50 ± 0.13
CrA IRS 7B	7.69 ± 0.02	0.16 ± 0.05	0.080 ± 0.019	2.2 ± 0.5	1.5 ± 0.5	3.1 ± 1.1	3.0 ± 1.2	0.19 ± 0.08
CrA IRAS 32	7.72 ± 0.04	0.09 ± 0.13	0.093 ± 0.018	1.4 ± 0.4	1.6 ± 0.2	3.5 ± 0.4	6.6 ± 2.5	0.12 ± 0.05
L1014 IRS	7.68 ± 0.01	0.19 ± 0.06	0.11 ± 0.022	3.7 ± 1.2	2.4 ± 0.7	5.1 ± 1.5	7.1 ± 2.3	0.53 ± 0.25
Average	7.69	0.16	0.10	2.7	1.5	4.1	5.8	0.34
Standard deviation	0.03	0.05	0.09	2.0	1.4	3.5	2.7	0.35

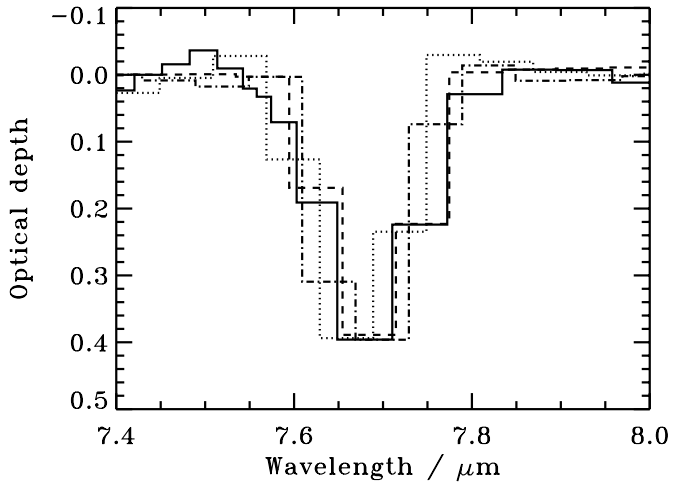

FIG. 3.—Optical depth spectra of B1-c (*solid line*) plotted together with laboratory spectra of a $CH_4:H_2O = 1:3$ mixture (*dashed line*), an $H_2O:CH_3OH:CO_2:CH_4 = 0.6:0.7:1:0.1$ mixture (*dotted line*), and pure CH_4 ice (*dot-dashed line*). The derived column densities using the three different ice compositions are 1.7×10^{18}, 1.6×10^{18}, and 1.7×10^{18} cm^{-2}, respectively.

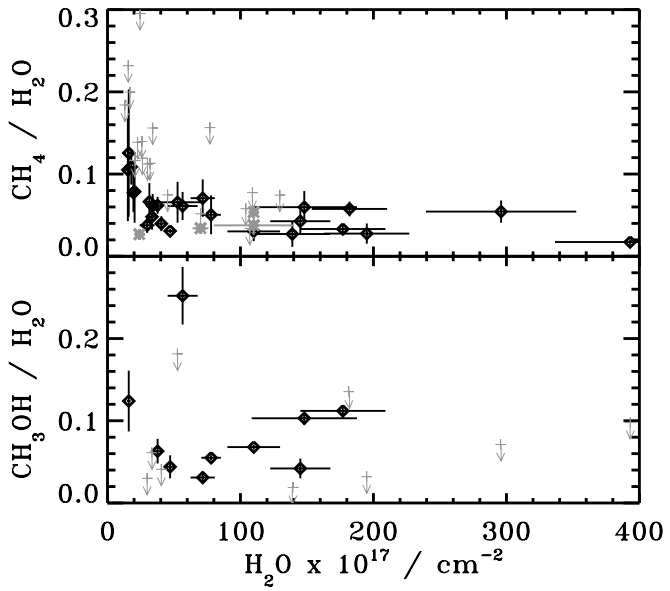

FIG. 4.—CH_4 and CH_3OH abundances relative to H_2O plotted vs. the column densities of H_2O for *Spitzer* IRS (*black diamonds*) and *ISO* (*gray asterisks*) CH_4 sources. Two groupings are visible in the top panel: sources with H_2O column densities around 2×10^{18} cm^{-2} with high CH_4 abundances, and sources with H_2O column densities of $(3–40) \times 10^{18}$ cm^{-2} and a nearly constant CH_4 abundance around 4%–5%. CH_3OH abundances show no similar groupings and span a larger interval than CH_4. CH_4 and CH_3OH abundance upper limits below 30% are plotted in gray.

in the high-abundance group, the uncertainties there tend to be larger. Below 3×10^{18} cm^{-2} there also seems to be some negative correlation between column density and CH_4 abundance. Figure 4 also shows the CH_3OH abundances and upper limits toward the sources in this sample (Paper I). CH_3OH abundances span a larger interval than CH_4 and show none of the column density dependencies visible for CH_4. The large variation for CH_3OH abundances is similar to what was found previously for a different sample by Pontoppidan et al. (2003).

The excess absorption (0%–55%) of the observed 7.7 μm features in many of the astronomical objects is due to broader profiles than expected even for CH_4 in an H_2O-rich ice. It is possible that an additional molecule is contributing to the optical depth of the 7.7 μm feature, e.g., solid SO_2. Solid SO_2 was suggested by Boogert et al. (1997) to explain the blue wing of the 7.7 μm feature in W33A. In contrast, another high-mass source, NGC 7538 IRS 9, displays no such wing. A comparison between these two sources and low-mass sources from this sample shows that the same variation is present here (Fig. 5): approximately 25% of the sources in this study have a clear blue wing, perhaps attributable to solid SO_2. The maximum amounts of SO_2 present in the observed ices are estimated by assuming that all excess absorption is due to SO_2 and using its measured band strength of 3.4×10^{-17} cm molecule^{-1} (Sandford & Allamandola 1993) (Table 2). The solid SO_2 abundances then vary between 0.1% and 1.5% with respect to H_2O.

In cases where the excess is similar on both sides of the CH_4 absorption, another source of the large widths of the features may be the choice of continuum; the spline continuum was difficult to fit because the CH_4 feature is generally shallow and overlapping with other, larger features. It is possible that the wings toward several sources are not intrinsic, but a product of this fit. This is highlighted by a comparison between Figures 1 and 2, which shows that the sources with clear continua also have thinner absorption features than the average.

3.2. *Upper Limits of Solid* CH_4

Upper limits for solid CH_4 were determined for the 27 sources without CH_4 detections, in the sample of 52 low-mass ice sources originally probed for CH_4, by estimating the maximum amount of an $H_2O:CH_4 = 3:1$ ice that could hide under the noise. The average 3 σ upper limit is 15% solid CH_4 with respect to solid H_2O, which is in the upper range of CH_4 abundances in the sources with solid CH_4 detections. All abundance upper limits below 30% are shown in Figure 4. Only one CH_4 upper limit, of ~3%, falls below the average abundance of 4.8%. The lack of detection in these 27 sources is hence probably due to the spectral quality and low fluxes of the objects rather than a lower amount of solid CH_4.

3.3. *Molecular Correlations*

The objects in this sample may vary significantly in temperature structure, as well as other environmental factors. Lack of correlations between molecular abundances may hence be due to either different formation pathways or differences in volatility. A lack of correlation between CH_4 and molecules of different volatility hence does not exclude that they formed in a similar manner. In pure form CH_4 has a similar volatility to CO (Collings et al. 2004). If CH_4 is mixed with H_2O, significant amounts can be trapped inside of the H_2O ice, however, and then CH_4 has an effective volatility closer to that of H_2O and CO_2.

The column densities of solid H_2O (26 detections) and CH_3OH (10 detections) have been derived in Paper I and those of solid CO (13 ground-based observations) and CO_2 (25 detections) have been derived in Pontoppidan et al. (2003) and Paper II for many of the CH_4 sources. The column densities and abundances for these molecules are plotted versus CH_4 in Figures 6 and 7. Where the plots reveal a linear relationship between molecules, the best linear fit is also drawn. The Pearson product-moment correlation coefficient, R, was calculated to measure the strength of the correlation: R^2 directly gives the fraction of variance of the second molecule that is due to changes in CH_4, assuming a linear relationship between the two molecules.

Figure 6 shows the correlations between the column densities of solid CH_4 and the four other ice components. Some correlation between column densities of ice species and total column density

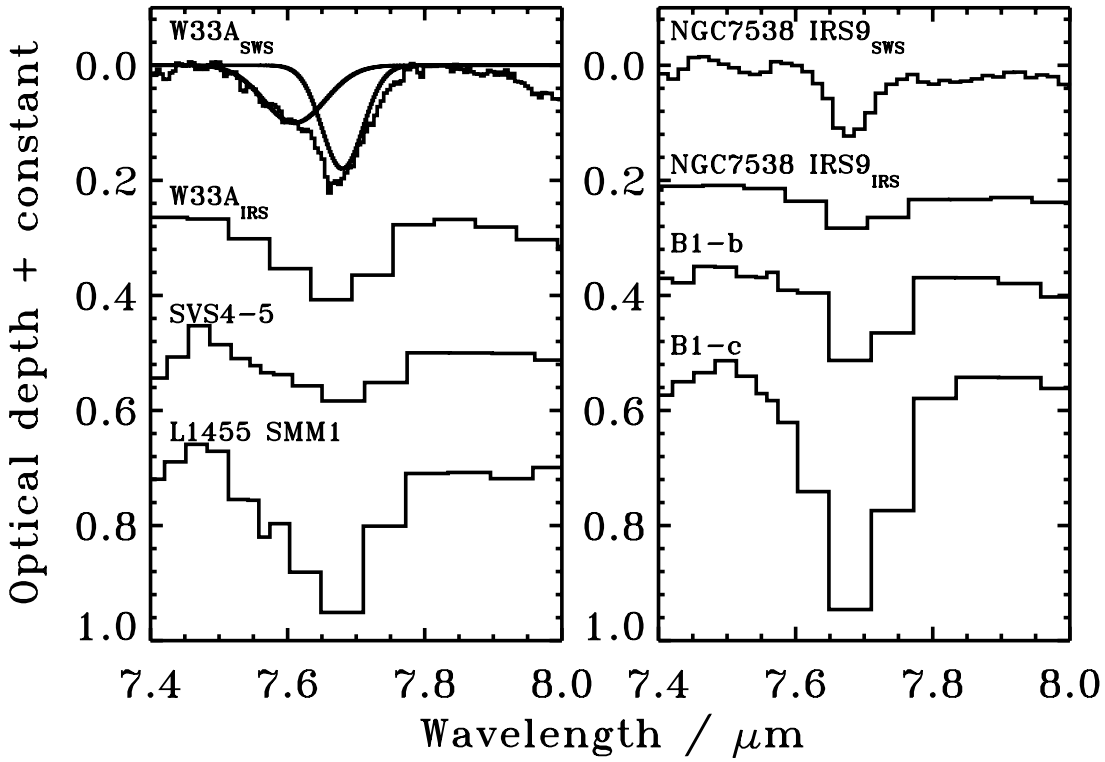

FIG. 5.—The 7.7 μm profile comparison between high-mass sources W33A and NGC 7538 IRS 9 (with their original SWS resolution and convolved to the resolution of IRS-SL1) and four low-mass sources. The two Gaussians plotted together with W33A fit the observed spectrum, but only the thin component centered at 7.7 μm is explained by CH_4. Several of the low-mass sources have similar profiles to W33A with an additional component, attributed to SO_2, that makes up the blue wing of the 7.7 μm feature. A few low-mass sources also show thin profiles similar to that of NGC 7538 IRS 9.

is always expected, but Figure 6 shows that the strength of this correlation is variable between CH_4 and the different molecules. CH_4 correlates strongly ($R^2 = 0.91$) with CO_2, which is believed to form on grain surfaces. The correlation with H_2O, another species formed on surfaces, is weaker ($R^2 = 0.64$), but this correlation coefficient is significantly increased if one outlier, IRAS 03245+3002, is removed. R^2 is then 0.82 for the CH_4-H_2O correlation. IRAS 03245+3002 could have been identified previous to the correlation studies as an outlier since it is the only source with no CO_2 ice detection, putting an upper limit on its CO_2/H_2O of 15%, compared to 30% $\pm$ 9% for the entire sample. Even without removing the outlier, the correlations are significant at the 99% level with 23 and 24 degrees of freedom (dof), respectively.

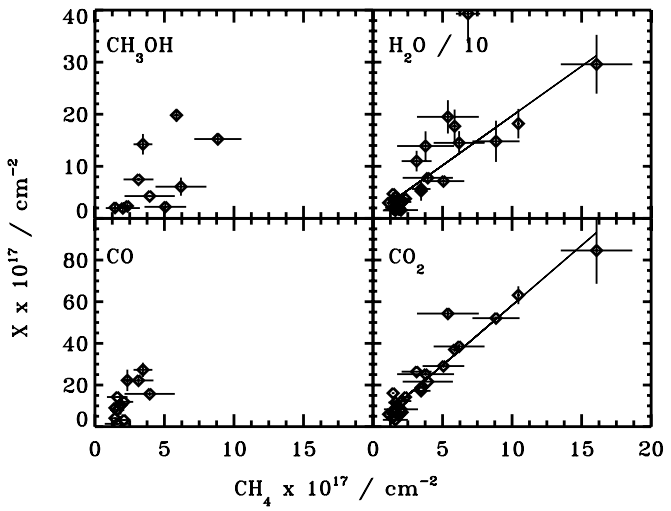

FIG. 6.—Column densities of four ice species, CH_3OH, H_2O, CO, and CO_2, plotted vs. the column densities of solid CH_4. Solid CH_4 is strongly correlated with solid CO_2 and H_2O. CH_4 is only weakly correlated with solid CO and CH_3OH, but this may be partly due to the fact that CO has only been observed and CH_3OH only detected toward much fewer targets. The outlier in the H_2O plot is IRAS 03245+3002.

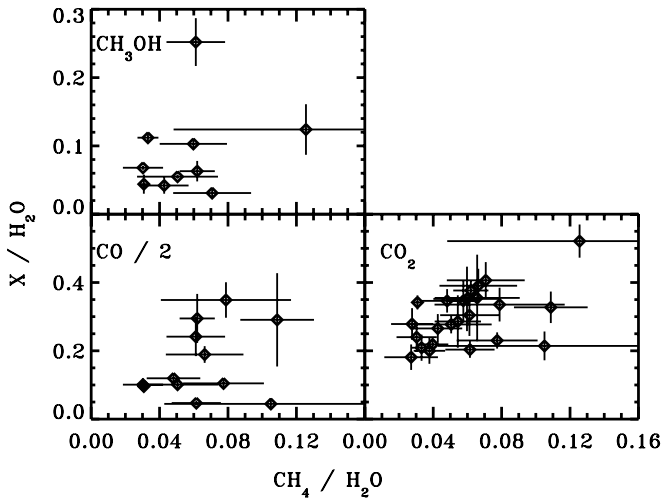

FIG. 7.—Abundances of solid CH_3OH, CO, and CO_2 relative to H_2O plotted vs. those of solid CH_4. There is no correlation between the relative amounts of solid CH_4 and CH_3OH or CO. In contrast, the CH_4 and solid CO_2 abundances are weakly correlated.

TABLE 3
AVERAGE CH_4 ABUNDANCE RELATIVE TO H_2O AND ITS STANDARD DEVIATION FOR FIVE OF THE INVESTIGATED CLOUDS AND FOR THE ENTIRE SAMPLE

Cloud	Number of Sources	Average	Standard Deviation
Perseus	6	0.040	0.014
Ophiuchus	6	0.083	0.019
B59.....	2	0.027	...
CrA.....	3	0.052	0.019
Serpens.....	2	0.093	...
All	25	0.058	0.027

CH_4 and CH_3OH and CO are barely significantly correlated ($R^2 = 0.48$ with 8 dof and 0.49 with 11 dof, respectively). The small number of CO abundances, which are only available for 11 of the targets in this study, complicates interpreting the low correlation plots between CO and CH_4. If only the sources for which CO measurements exist are used to calculate the CH_4-CO_2 and CH_4-H_2O correlations, these are reduced to $R^2 = 0.57$ and 0.59, respectively.

The stronger correlation between CH_4 and CO_2 compared to CH_4 and H_2O is curious, but may be an artifact of the fact that the CO_2 column densities are better known for this sample than the H_2O column densities. For most sources in this sample the H_2O column densities are determined by estimating the depth of the H_2O libration feature, which is difficult due to the overlap with the silicate feature at 9.7 μm. The uncertainties in these H_2O column densities were estimated to $\sim$30% in Paper I after comparison between derived abundances from the 3 μm mode and the libration mode for the sources with 3 μm spectra. Furthermore, the different amounts of CO_2 toward the different sources may introduce further error in the derived H_2O column densities as recently shown in Öberg et al. (2007).

Figure 7 shows the correlations between solid CH_4 and the other three ice species, with the abundances normalized to the solid H_2O column density, the main ice constituent (Fig. 7). When normalizing to H_2O, there is no significant correlation at a 95% level between CH_4 and CH_3OH and CO (R^2 below 0.1) and at best a weak correlation between CH_4 and CO_2 ($R^2 = 0.27$). There is also no correlation between CH_4 abundances and any of the three CO components as defined by Pontoppidan et al. (2003), with the different components corresponding to pure CO and CO in an H_2O- and CO_2-rich ice, respectively.

3.4. *Spatial Trends*

The average CH_4 abundance relative to H_2O and its standard deviation are shown for all clouds with more than one detection and for the entire sample in Table 3. The averages for the individual clouds range from 2.8% to 9%, with Serpens and Ophiuchus at 9% and 8%, respectively. Whether the clouds are significantly different in their CH_4 abundances was evaluated using Analysis of Variance with the Statistics101 resampling software. Resampling is more robust than traditional statistical tests since there is no need to assume an underlying distribution, which is especially useful when the sample size is small. The test procedure starts with calculating the sum of the absolute deviations of the cloud averages from the sample average. The CH_4 abundances in the five clouds are then randomly resampled into five new groups with the same group size distribution as before, and the absolute deviations of the group averages from the sample average are recalculated. This is repeated 1000 times, and the number of times the resampled sum of deviations exceeds the sum of deviations of the cloud averages is counted. The null hypothesis that the difference between the clouds is due to chance could then be rejected with 95% confidence. If Ophiuchus is removed from the sample, there are no longer any significant differences between the clouds.

4. DISCUSSION

4.1. *Low- versus High-Mass YSOs*

For comparison the solid CH_4 abundances with respect to H_2O for several high-mass YSOs (Table 1) were rederived and plotted relative to H_2O abundances from Gibb et al. (2004) in Figure 4. These sources have been previously investigated for solid CH_4 by Boogert et al. (1996) and Gibb et al. (2004). The solid CH_4 abundances derived here are 30%–60% higher than those published by Gibb et al. (2004) mainly due to a difference in band strength (Gibb et al. 2004: 7.3×10^{-18} molecules cm^{-1}; this paper: 4.7×10^{-18} molecules cm^{-1}). The plot shows that the high-mass *ISO* CH_4 sources fit in seamlessly with the low-mass CH_4 sources with H_2O column densities above 2×10^{18} cm^{-2}. Figure 5 also shows that there is a similar variation in the 7.7 μm feature profile between low- and high-mass objects. There is hence no reason to expect large systematic differences in CH_4 abundances or formation pathways toward low- and high-mass YSOs.

4.2. *Formation Scenarios*

The similar or higher abundance of CH_4 with respect to H_2O toward the low-mass sources in this sample compared to what has been found previously toward high-mass YSOs suggests that the CH_4 formation rate is not dependent on stellar UV irradiation. Of the three formation scenarios for CH_4 suggested in the introduction, this study hence does not support a formation pathway connected to stellar UV processing of CH_3OH. Furthermore, in the sources with $(2–40) \times 10^{18}$ cm^{-2} H_2O the CH_4 abundance is nearly constant. In comparison, the CH_3OH abundances vary by a factor of 10, and it seems unlikely that this would be the outcome if the main formation pathway of CH_4 is connected to CH_3OH through, e.g., cosmic-ray–induced UV processing of CH_3OH, which is also present under quiescent conditions.

Of the two remaining scenarios, formation in the gas phase with subsequent freezeout and hydrogenation of C on grain surfaces, this study lends most support to the latter mechanism. First, under quiescent conditions, gas-phase models predict steady state total CH_4/H_2 abundances of only around 10^{-7} to 5×10^{-14} (Woodall et al. 2007; Bergin et al. 1995), compared with our inferred CH_4/H_2 abundances of $\sim(2–13) \times 10^{-6}$ (assuming a standard H_2O/H_2 ratio of 10^{-4}). In early times when C/CO > 1, the CH_4/H_2 can reach above 10^{-6} (Millar et al. 1991). Ices cannot form at extinctions lower than $\sim 2A_V$, however (Cuppen & Herbst 2007). At extinctions higher than $2A_V$, C/CO < 1 and hence freezeout of the high CH_4 abundances at early times cannot be used to explain the high ice abundances. In addition, pure CH_4 has a similar volatility to CO, within a few degrees (Collings et al. 2004), and if both are formed in the gas phase and subsequently frozen out, the two molecules should correlate, both in absolute column densities and in abundances relative to the much less volatile H_2O. This study clearly shows that this is not the case.

This weak correlation between CO and CH_4 can be contrasted with the stronger correlations between CH_4 and CO_2 and H_2O column densities. Furthermore, the lack of significant correlation with any species once the correlation with H_2O has been effectively divided out, by normalizing with the H_2O column densities, shows that CH_4 is not significantly better related to

any other molecule than to H_2O. Together this suggests a formation scenario of CH_4 more related to H_2O and CO_2 formation, which both form on grains, rather than to CO. In theory the correlations could be single-handedly due to the fact that CH_4 has a higher desorption temperature than in its pure form due to mixing with H_2O. This, however, is only expected to occur if CH_4 is formed together with H_2O; hence, CH_4 formation on grain surfaces is still the most plausible outcome of this study.

The hydrogenation scenario is also supported by the broad profiles of the features that have only been found in laboratory spectra when CH_4 is in a mixture with hydrogen-bonding molecules, which are believed to form on grain surfaces. These conclusions are in agreement with studies of the solid CH_4 profiles toward high-mass YSOs, which show that solid CH_4 is mixed with H_2O or possibly CH_3OH (Boogert et al. 1997) and also with the observed low gas/solid ratio of CH_4 compared to CO (Boogert et al. 2004a).

4.3. *Differences between Clouds*

Figure 4 and Table 3 show that the CH_4 abundances differ from cloud to cloud. In Figure 4, four of the five sources with high CH_4 abundances and H_2O column densities below 2×10^{18} cm^{-2} are Ophiuchus sources (the fifth is in Serpens). The two Ophiuchus sources that have higher H_2O ice abundances also have more "normal" CH_4 abundances. This indicates that it is the low total column density toward four of the Ophiuchus sources, rather than initial conditions in Ophiuchus as a whole, that is responsible for the extreme CH_4 abundances found there. This may be due to the fact that toward sources with low total column densities the C/CO ratio may be larger, allowing for more CH_4 to form. The C/CO ratio is dependent on extinction for low extinctions, but not for high ones. This is consistent with our observation that CH_4 abundances are only dependent on total column densities for low column densities. Sakai et al. (2008) have instead suggested that different CH_4 abundances could be due to different collapse times. In clouds that collapse very fast, chemical equilibrium may not be reached, favoring a C-based rather than CO-based chemistry. This question can only be settled if gas-phase data for these sources become available.

4.4. *Comparison with Models*

Solid CH_4 abundances have been modeled previously for a variety of conditions (Hasegawa et al. 1992; Aikawa et al. 2005). The predicted CH_4 ice abundances with respect to H_2O usually vary between $\approx$1% and 10%, with the main formation path being sequential hydrogenation of C atoms on grains at a time when a large fraction of the gas-phase C has already been converted to CO, i.e., C/CO < 1. The observed abundances in our sample fall mostly within this range and are hence in general agreement with the models.

Aikawa et al. (2005) model molecular abundances on grain surfaces and in the gas phase during the collapse of a spherical cloud. Regardless of initial conditions and the central density when the collapse is stopped, the CH_4/H_2O and CH_4/CO_2 ice ratios are fairly constant as a function of radius in the cloud. The value of CH_4/H_2O ratio varies with initial conditions between a few and 10%. In contrast, the CH_4/CO ratio is radius dependent. The model of Hasegawa et al. (1992) is more aimed at modeling interstellar clouds before collapse, but as they show the time evolution of the chemistry, it may still be useful to compare with our observations. As in the collapse model, CH_4, CO_2, and H_2O trace each other fairly well, while CO and CH_4 are only correlated during some time intervals, regardless of initial conditions. Both these models are consistent with Figure 6, where solid CH_4 is better correlated with H_2O and CO_2 than with CO.

5. CONCLUSIONS

We present *Spitzer* IRS spectra of the solid CH_4 feature at 7.7 μm toward a large sample of low-mass YSOs. Our conclusions are as follows:

1. A total of 25 out of 52 low-mass YSOs show a solid CH_4 feature at 7.7 μm.
2. The solid CH_4 abundance with respect to H_2O is centered at 5.8% with a standard deviation of 2.7% in the sources with CH_4 detections. In the sources without detections the average upper limit is 15%, which is not significant compared with the detections.
3. The sources (two Ophiuchus and one Serpens) with more than 10% CH_4 all have H_2O column densities below 2×10^{18} cm^{-2}. Due to the low total column densities, two of these three sources have uncertainties larger than 50%. Above 2×10^{18} cm^{-2} the sources (20 out of 25) have a fairly constant CH_4 abundance of 4.7% $\pm$ 1.6%.
4. The 7.7 μm feature profiles are significantly broader for all but one object than expected for pure solid CH_4 and toward most sources also broader than expected for CH_4 in H_2O-dominated ices. Approximately 30% of the features have a blue wing, seen previously toward high-mass YSOs and there attributed to solid SO_2.
5. The column densities of solid CH_4 and H_2O and CO_2 are clearly correlated, while CH_4 and CO and CH_3OH are only weakly correlated.
6. There is also no correlation between the CH_4 and CO abundances when both have been normalized to the H_2O abundance.
7. The Ophiuchus cloud has significantly higher CH_4 abundances compared to the rest of the sample, probably due to the low total column densities toward several of the sources. There are no significant differences between the remaining clouds.
8. The abundance variation is smaller for CH_4 compared to solid CH_3OH; CH_4 seems to belong to the class of molecules, also including H_2O and CO_2, that appear "quiescent," i.e., their abundances are more or less constant, in contrast to highly variable ices like CH_3OH and OCN^-. If the Ophiuchus sources are included, CH_4 is somewhere between the two classes.
9. Sample statistics and comparison with model predictions support CH_4 formation through hydrogenation of C on grain surfaces.

We thank Claudia Knez and the *Spitzer* c2d IRS team for useful comments on the manuscript. Funding for K. I. Ö. and E. F. v. D. was provided by NOVA, the Netherlands Research School for Astronomy, a grant from the European Early Stage Training Network (MEST-CT-2004-504604), and an NWO Spinoza grant. Support for K. M. P. was provided by NASA through Hubble Fellowship grant 1201.01 awarded by the Space Telescope Science Institute, which is operated by the Association of Universities for Research in Astronomy, Inc., for NASA, under contract NAS 5-26555.

REFERENCES

Aikawa, Y., Herbst, E., Roberts, H., & Caselli, P. 2005, ApJ, 620, 330
Alexander, R. D., Casali, M. M., André, P., Persi, P., & Eiroa, C. 2003, A&A, 401, 613
Allamandola, L. J., Sandford, S. A., & Valero, G. J. 1988, Icarus, 76, 225
Allen, M., & Robinson, G. W. 1977, ApJ, 212, 396
Bergin, E. A., Langer, W. D., & Goldsmith, P. F. 1995, ApJ, 441, 222
Boogert, A. C. A., Blake, G. A., & Öberg, K. 2004a, ApJ, 615, 344
Boogert, A. C. A., Helmich, F. P., van Dishoeck, E. F., Schutte, W. A., Tielens, A. G. G. M., & Whittet, D. C. B. 1998, A&A, 336, 352
Boogert, A. C. A., Schutte, W. A., Helmich, F. P., Tielens, A. G. G. M., & Wooden, D. H. 1997, A&A, 317, 929
Boogert, A. C. A., Tielens, A. G. G. M., Ceccarelli, C., Boonman, A. M. S., van Dishoeck, E. F., Keane, J. V., Whittet, D. C. B., & de Graauw, T. 2000, A&A, 360, 683
Boogert, A. C. A., et al. 1996, A&A, 315, L377
———. 2004b, ApJS, 154, 359
———. 2008, ApJ, 678, 985 (Paper I)
Brown, P. D., Charnley, S. B., & Millar, T. J. 1988, MNRAS, 231, 409
Cernicharo, J., Noriega-Crespo, A., Cesarsky, D., Lefloch, B., González-Alfonso, E., Najarro, F., Dartois, E., & Cabrit, S. 2000, Science, 288, 649
Collings, M. P., Anderson, M. A., Chen, R., Dever, J. W., Viti, S., Williams, D. A., & McCoustra, M. R. S. 2004, MNRAS, 354, 1133
Cuppen, H. M., & Herbst, E. 2007, ApJ, 668, 294
Dartois, E., Muñoz Caro, G. M., Deboffle, D., Montagnac, G., & D'Hendecourt, L. 2005, A&A, 432, 895
Dartois, E., Schutte, W., Geballe, T. R., Demyk, K., Ehrenfreund, P., & D'Hendecourt, L. 1999, A&A, 342, L32
Evans, N. J., II, et al. 2003, PASP, 115, 965
Gerakines, P. A., Schutte, W. A., & Ehrenfreund, P. 1996, A&A, 312, 289
Gerakines, P. A., et al. 1999, ApJ, 522, 357
Gibb, E. L., Whittet, D. C. B., Boogert, A. C. A., & Tielens, A. G. G. M. 2004, ApJS, 151, 35
Gürtler, J., Klaas, U., Henning, T., Ábrahám, P., Lemke, D., Schreyer, K., & Lehmann, K. 2002, A&A, 390, 1075
Hasegawa, T. I., Herbst, E., & Leung, C. M. 1992, ApJS, 82, 167
Hiraoka, K., Miyagoshi, T., Takayama, T., Yamamoto, K., & Kihara, Y. 1998, ApJ, 498, 710
Keane, J. V., Tielens, A. G. G. M., Boogert, A. C. A., Schutte, W. A., & Whittet, D. C. B. 2001, A&A, 376, 254
Knez, C., et al. 2005, ApJ, 635, L145
Lacy, J. H., Carr, J. S., Evans, N. J., II, Baas, F., Achtermann, J. M., & Arens, J. F. 1991, ApJ, 376, 556
Markwick, A. J., Millar, T. J., & Charnley, S. B. 2000, ApJ, 535, 256
Millar, T. J., Bennett, A., Rawlings, J. M. C., Brown, P. D., & Charnley, S. B. 1991, A&AS, 87, 585
Öberg, K. I., Fraser, H. J., Boogert, A. C. A., Bisschop, S. E., Fuchs, G. W., van Dishoeck, E. F., & Linnartz, H. 2007, A&A, 462, 1187
Pontoppidan, K. M., Dartois, E., van Dishoeck, E. F., Thi, W.-F., & d'Hendecourt, L. 2003, A&A, 404, L17
Pontoppidan, K. M., et al. 2008, ApJ, 678, 1005 (Paper II)
Sakai, N., Sakai, T., Hirota, T., & Yamamoto, S. 2008, ApJ, 672, 371
Sandford, S. A., & Allamandola, L. J. 1993, Icarus, 106, 478
Tielens, A. G. G. M., & Hagen, W. 1982, A&A, 114, 245
van de Hulst, H. C. 1946, Rech. Astron. Obs. Utrecht, 11, 2
Woodall, J., Agúndez, M., Markwick-Kemper, A. J., & Millar, T. J. 2007, A&A, 466, 1197
Young, C. H., et al. 2004, ApJS, 154, 396